A Numerical Approach to the Geometry of Ciliary Dynamics

by

Amalia Culiuc

Research advisor:

Prof. Mark Peterson

A thesis submitted in partial fulfillment

of the requirements for the degree of

Bachelor of Arts with Honors in Mathematics

Mount Holyoke College,

South Hadley, MA

May 1, 2011

I give permission for public access to my thesis and for any copying to be done at the discretion of the archives librarian and/or the College librarian.

Amalia Viorela Culiuc

May 1, 2011

Acknowledgements

I thank my thesis advisor, Professor Mark Peterson, for all his help and guidance and for introducing me to this problem. My gratitude to my thesis committee, Professor Janice Gifford and Professor Stan Rachootin, for their time and support and for agreeing to read this paper and provide feedback; the Mount Holyoke College mathematics and statistics department, especially Professors Giuliana Davidoff, Alan Durfee, Harriet Pollatsek, Margaret Robinson for being the best mentors and role models a student could hope for; my academic advisor, Professor Jessica Sidman, for her advice, her support and for believing in me more than I ever believed in myself. I hope I haven't disappointed her; the UMass Amherst mathematics department for all the background they have helped me acquire; Professor Thomas Witelski from Duke University for his lecture on the calculus of variations; Michael Casey from Princeton University for offering some of the references and helping me understand them better; Mark Lowell from UMass Amherst for his quick introduction to tensors and manifolds; Professor William Davis and Dr. Patrick Sears from the University of North Carolina Medical School for providing videos and data on the human respiratory cilia.

I would also like to thank all the great people who have encouraged and advised me during these four years: my REU mentors, Professor Sivaram Narayan and Professor Mihai Stoiciu, my friends, and most importantly my family.

Abstract

The motion of cilia and flagella under internal stresses has been widely studied over the past years as a way of relating the biology of these structures and the functions they perform. While the mechanism which leads to the ciliary motion is fairly well understood, its method of activation and coordination is still essentially unknown. In this paper, we present a geometric approach to modeling ciliary dynamics which suggests that the motion of a free flowing cilium can be completely described by its shape. We then introduce the numerical method of least squares piecewise polynomial projections as a potential tool for solving the systems of partial differential equations in the ciliary dynamics models. It is concluded that although stability issues arise, with some adjustments, the method could potentially be employed with success: it is possible to create computer simulations of the motion predicted by this geometric model and the results are expected to provide a good match for the biological data.

Contents

Acknowledgements **2**

Abstract **3**

1 Introduction **5**

2 The Geometric Model **7**

2.1 Metric Relations in the Ciliary Material 8

2.2 Ciliary Flow and Dynamics 15

2.3 Phenomenological Energy and Interior Forces 17

2.4 The Net Force Condition 20

3 Numerical Approximations - Finite Elements Methods **23**

3.1 Least Squares Projection into Piecewise Polynomial Spaces . . 24

3.2 Projecting in V_J^n 30

3.3 The Heat Equation 36

3.4 Solving $\Lambda_{xx} = g\Lambda + h$ 41

4 Two-dimensional Ciliary Motion **43**

A Conditions for Ciliary Flows **48**

B Variational Derivatives of Elastic Energy **51**

1 Introduction

Cilia are slender motile organelles found in eukaryotic cells, from protozoans to mammals and even some plants. In humans they are present for example in the cells lining the trachea, and help sweep foreign particles away from the lungs. Structurally, cilia are essentially identical to flagella, differing only in length and sometimes in the function they perform. While cilia can be locomotive or sensory organelles, the flagella's function is primarily locomotion.

The internal structure of the cilium, seen in cross section, consists of a central pair of microtubules with 9 outer doublet microtubules disposed in a circle [6], as shown in Figure 1.

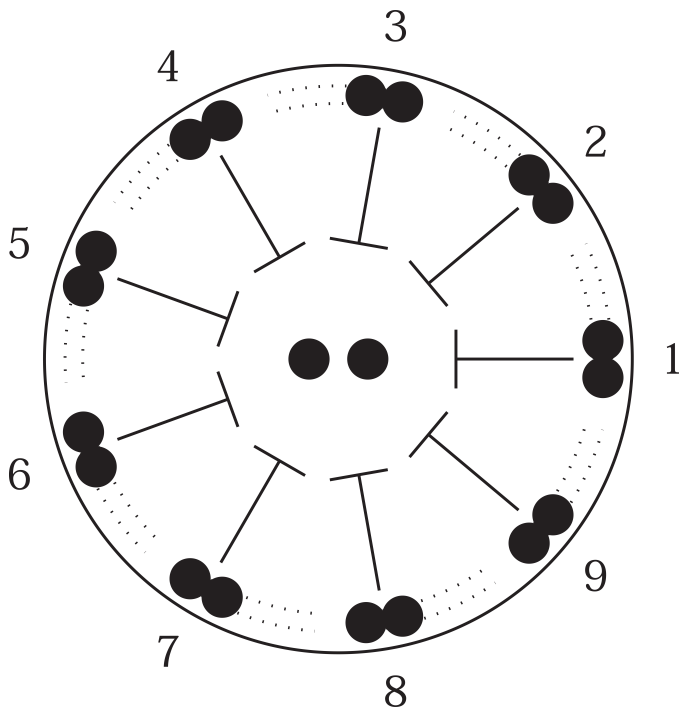

Figure 1: Cross section of a cilium [7] displaying the arrangement of the 9 doublet microtubules and the central pair. The dynein is represented by dots connecting the doublets

Adjacent microtubules are bound through axonemal dynein, a motor protein that facilitates the transversal shearing of the doublets against each other. When the dynein gets activated, it "walks" along the microtubules causing them to slide. However, in order to permit the back and forth motion, it is necessary that the activation and inactivation of the dynein molecules be coordinated on diametrally opposite sides.

Radial spokes are present as part of a linkage mechanism connecting the central pair to the outer doublets. One of the roles that the spokes play is to hold the microtubules in place so that the sliding can only be done longitudinally, imposing a constraint on the range of motion. Although it has been found from experimental data that the composition of the spokes determine the ciliary beating pattern, there is not much information available about the action of these proteic structures [5]. What is known is that the longitudinal shearing leads to the bending of the cilium and thus to the characteristic beat.

Even though the mechanism of ciliary motion is generally agreed upon and has been widely studied, the coordination in the activation and deactivation of the dynein that leads to the bending of the organelle is still far from being understood. One difficulty is that the motion itself differs from one organism to another. For instance, in the human tracheal lining cells, the beat is planar, but in paramecia or in trypanosoma, the movement is effectively three-dimensional. The manner in which the dynein arms are activated and deactivated to lead to specific beats constitutes a challenge in modeling ciliary dynamics, which we approach in the present work.

The rest of the paper is structured as follows: in Section **2** we describe the mathematical model, as developed in [7], imposing the necessary biological and

physical constraints. The key observation in this model is the coupling of shear strain and bending, which implies that the shape of the cilium can be found by a basic integration of the strain function. In order to solve the equations that arise and to perform the required integration, in Section **3** we introduce the numerical method of finding solutions to partial differential equations through finite element least squares projections into piecewise polynomial spaces. We study the benefits and constraints of this method by employing it to solve well understood equations, such as the heat flow, which leads to questions of stability and projection degrees of freedom. In Section **4**, we show how the piecewise polynomial method can be employed to create numerical simulations of the motion of cilia and flagella under internal stresses. We conclude that while there are still important stability issues to be resolved, the method is conceptually well suited for solving large partial differential equation systems and thus may be employed successfully to obtain computer simulations of mathematical models of ciliary geometry.

2 The Geometric Model

In this section, we outline the model described in [7] following the original notation. It is known that despite the various bending patterns corresponding to different species, all cilia obey the same set of biological constraints: they are inextensible, incompressible in all directions, and the shear strain is only exhibited along the filaments[7]. Phrased differently, the length and width of the organelle are not changed through bending, and the strain manifests itself only longitudinally.

2.1 Metric Relations in the Ciliary Material

Assume initially that the cilium is made out of an incompressible, inextensible "ciliary material" whose particles move in a coordinate system (x^1, x^2, x^3). Then the change of position of a particle along the direction x^i is described by

$$\frac{dx^i}{dt} = V^i(x, t),$$

where V is the velocity vector and V^i is its component in the direction x^i. In the two dimensional case, the distance between two particles, defined using the Einstein convention, follows the relation:

$$ds^2 = g_{ij}dx^i dx^j. \tag{1}$$

Here g_{ij} is the metric tensor, a generalization of the concept of distance on a manifold, and ds, known as the line element, expresses the said distance. The Einstein convention is simply a shortened method of notation, which states that if an index appears twice in a single term, it stands for the summation over all indices.

In very general terms, the metric tensor is a symmetric matrix whose entries measure distances in a coordinate system of arbitrary dimensions. Its components can be seen as multiplication constants in the generalized Pythagorean theorem. In other words, the notation in equation (1) stands for the statement that

$$ds^2 = g_{11}d(x^1)^2 + 2g_{12}dx^1dx^2 + g_{22}d(x^2)^2.$$

For instance, in the Euclidean geometry on a plane, the metric tensor has the

form

$$g = \begin{pmatrix} 1 & 0 \\ 0 & 1 \end{pmatrix}$$

which implies that

$$ds^2 = dx^2 + dy^2,$$

or, equivalently,

$$s = \int_\alpha^\beta \sqrt{dx^2 + dy^2},$$

the known formula for calculating arc length.

The off-diagonal symmetry of the matrix g comes from the fact that in any coordinate system, the distance from a point α to a point β should always equal the distance from β to α.

Returning to the ciliary geometry, instead of viewing the displacement as a change in coordinates, let every point preserve its coordinates and let the coordinate system itself be displaced. Then the metric in this coordinate system will change in time, at a rate given by the Lie derivative of the metric tensor g:

$$\frac{\partial g_{jk}}{\partial t} = \mathcal{L}_v g(\partial_j, \partial_k) = V g_{jk} + g([\partial_j, V], \partial_k) + g(\partial_j, [\partial_k, V]) \tag{2}$$

To show how equation (2) can be used to compute the metric, we provide an example that is also described in [7]. Consider a planar motion due to a flow

$$V = yS\partial_x,$$

where S is a constant shear strain and the coordinate system begins as carte-

sian coordinates x and y. Then at any time t, g can be represented by its Lie-Taylor series as follows

$$g(t) = g(0) + t\mathcal{L}_v g(0) + \frac{t^2}{2!}\mathcal{L}_v\mathcal{L}_v g(0) + \frac{t^3}{3!}\mathcal{L}_v\mathcal{L}_v\mathcal{L}_v g(0) + ...$$

where

$$g(0) = \begin{pmatrix} 1 & 0 \\ 0 & 1 \end{pmatrix}.$$

By the definition of V, $[\partial_x, V] = 0$ and $[\partial_y, V] = S\partial_x$. Thus

$$\mathcal{L}_v g(0) = \begin{pmatrix} 0 & S \\ S & 0 \end{pmatrix}.$$

Furthermore,

$$\mathcal{L}_v\mathcal{L}_v g(0) = \begin{pmatrix} 0 & 0 \\ 0 & S^2 \end{pmatrix},$$

and

$$\mathcal{L}_v\mathcal{L}_v\mathcal{L}_v g(0) = \begin{pmatrix} 0 & 0 \\ 0 & 0 \end{pmatrix}.$$

Then the Taylor series terminates and we have that

$$g(t) = \begin{pmatrix} 1 & 0 \\ 0 & 1 \end{pmatrix} + \begin{pmatrix} 0 & St \\ St & 0 \end{pmatrix} + \begin{pmatrix} 0 & 0 \\ 0 & S^2t^2 \end{pmatrix} = \begin{pmatrix} 1 & St \\ St & S^2t^2 + 1 \end{pmatrix}$$

So at time $t = 1$, the metric tensor g is

$$g = \begin{pmatrix} 1 & S \\ S & 1 + S^2 \end{pmatrix}$$

This expression allows us to calculate distances using the generalized Pythagorean theorem. Suppose the displacement is from $(0, 0)$ to $(1, 1)$, as in Figure 2.

Then it is easy to see that the Euclidean distance between the points is $\sqrt{(S+1)^2 + 1}$. Using the metric tensor,

$$\begin{aligned} ds^2 &= g_{11}d_x^2 + 2g_{12}d_x d_y + g_{22}d_y^2 \\ &= 1 \cdot 1 + 2 \cdot S \cdot 1 \cdot 1 + (1 + S^2) \cdot 1 \\ &= S^2 + 2S + 2 \\ &= (\sqrt{(S+1)^2 + 1})^2 \end{aligned}$$

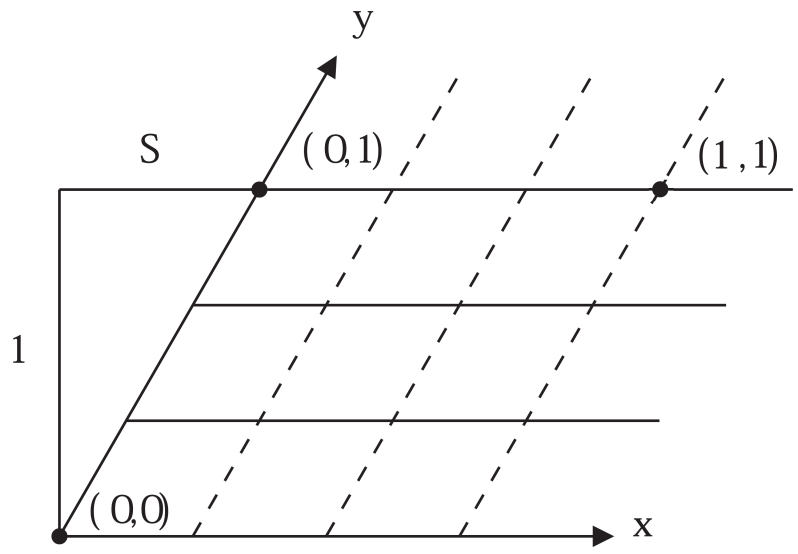

Figure 2: In this skew coordinate system [7], the metric tensor provides a way to calculate Euclidean distances that is equivalent to the Pythagorean theorem result

Note that since the x direction is chosen to be the direction along the filament, if there is no displacement dy, then

$$ds^2 = g_{11}d_x^2 = d_x^2, \tag{3}$$

so g_{11} has to equal 1 if the filament is inextensible.

The three dimensional generalization, also described in [7], depends on two components of the shear strain, the longitudinal strain S and the normal strain, T. In this case, through a similar derivation as in the two-dimensional system,

$$g = \begin{pmatrix} 1 & S & T \\ S & 1+S^2 & ST \\ T & ST & 1+T^2 \end{pmatrix}. \tag{4}$$

To the metric g we associate an orthonormal frame (e_1, e_2, e_3) described by

$$e_1 = \partial_x \tag{5}$$

$$e_2 = \partial_y - S\partial_x \tag{6}$$

$$e_3 = \partial_z - T\partial_x \tag{7}$$

The notation (e_1, e_2, e_3) will play a dual role, representing both a set of orthonormal vectors for a given filament and a set of vector fields whose components create orthonormal triplets for each filament. The meaning should be clear from the context and should not lead to any ambiguity.

As a vector field, e_1 is the field of unit vectors following the direction tangent to a filament. Then if y and z represent the direction of motion of adjacent filaments, e_2 and e_3 are orthogonal to e_1.

The rate of change of e_2 and e_3 along the tangent to the filament are given by

the Lie brackets (the "directional derivatives in the direction of e_1"):

$$\partial_x e_2 = [e_1, e_2] = -S_x e_1 \tag{8}$$

$$\partial_x e_3 = [e_1, e_3] = -T_x e_1 \tag{9}$$

Then, by the Frenet equations, the curvature vector is

$$\kappa \hat{N} = \partial_x e_1 = S_x e_2 + T_x e_3,$$

where $\hat{N}$ is the unit normal and, by finding the norm in the expression above,

$$\kappa = \sqrt{S_x^2 + T_x^2}. \tag{10}$$

The binormal is defined as

$$\hat{B} = \hat{T} \times \hat{N} = \begin{vmatrix} e_1 & e_2 & e_3 \\ 1 & 0 & 0 \\ 0 & \frac{S_x}{\kappa} & \frac{T_x}{\kappa} \end{vmatrix} = \frac{e_3 S_x - e_2 T_x}{\kappa},$$

so the torsion is obtained by computing the dot product of the rate of change of the normal in the direction of the filament and the binormal:

$$\begin{aligned} \tau &= [e_1, \hat{N}] \cdot \hat{B} \\ &= \left(\frac{S_{xx} e_2 - S_x^2 e_1 + T_{xx} e_3 - T_x^2 e_1}{\kappa} \right) \cdot \left(\frac{e_3 S_x - e_2 T_x}{\kappa} \right) \\ &= \frac{T_{xx} S_x - S_{xx} T_x}{\kappa^2}. \end{aligned}$$

To obtain an intuition about the geometry, it may be more useful to convert the Frenet description into a description that is closely related to the properties of

the cilium. From the expressions for curvature and torsion, through a convenient parametrization, we have:

$$S_x = \kappa \cos\phi$$

$$T_x = \kappa \sin\phi$$

$$\phi_x = \tau.$$

The angle ϕ, whose rate of change gives the torsion, is the "twisting angle". The fact that ϕ is so loosely defined is not unintentional, but a result of an essential property of the (e_1, e_2, e_3) system: while $\hat{N}$ and $\hat{T}$ have clearly determined directions in space, all that is required for e_2 and e_3 is that they be perpendicular to e_1, which leads to the conclusion that their directions are only determined up to a rotation about e_1.

If the filament shape is parameterized by a space curve $\overrightarrow{R}(x)$, then

$$\overrightarrow{R}_x = e_1$$

Also, substituting the expressions for S_x and T_x into equations (8)-(9)

$$\partial_x e_2 = -\kappa \cos\phi e_1$$

$$\partial_x e_3 = -\kappa \sin\phi e_1.$$

Thus, the geometry of the filament is described by the following set of equations

$$\overrightarrow{R}_x = e_1 \tag{11}$$

$$\partial_x e_1 = \kappa \cos\phi e_2 + \kappa \sin\phi e_3 \tag{12}$$

$$\partial_x e_2 = -\kappa \cos\phi e_1 \tag{13}$$

$$\partial_x e_3 = -\kappa \sin\phi e_1 \tag{14}$$

$$\phi_x = \tau \tag{15}$$

2.2 Ciliary Flow and Dynamics

We now introduce the ciliary flow, as described in [7]. Let V be the flow of the ciliary material obeying the biological constraints. Then, by the definition of the ciliary flow, V must preserve the form of g from equation (4). Let V be defined as

$$V = \alpha\partial_x + \beta\partial_y + \gamma\partial_z.$$

By equations (5)-(7), it results that

$$V = \alpha e_1 + \beta(e_2 + Se_1) + \gamma(e_3 + Te1) \tag{16}$$

$$= (\alpha + \beta S + \gamma T)e_1 + \beta e_2 + \gamma e_3 \tag{17}$$

In order to satisfy the inextensibility assumption, the metric tensor g must fulfill the condition $g_{11} = 1$ at all times, as it has been shown to happen in equation (3) for a particular example. Therefore, from equation (2), since g_{11} is constant,

$$\partial_t g_{11} = \mathcal{L}_V g(\partial_1, \partial_1) = V g_{11} + g([\partial_x, V], \partial_x) + g(\partial_x, [\partial_x, V]) = 0.$$

so it is necessary to impose the condition

$$2g([\partial_x, V], \partial_x) = 2g(\alpha_x\partial_x + \beta_x\partial_y + \gamma_x\partial_z, \partial_x) = 2(\alpha_x + S\beta_x + T\gamma_x) = 0 \tag{18}$$

Other conditions required by the fact that V preserves g are derived in appendix A:

$$0 = e_2\beta \tag{19}$$

$$0 = e_3\gamma \tag{20}$$

$$0 = e_2\gamma + e_3\beta \tag{21}$$

Furthermore, in spite of the unusual coordinates, the space we are describing is still the Euclidean space (at any moment in time, the distances between points are Euclidean distances). Thus, the space must maintain zero Riemannian curvature. As proved in [7] using equation (21), in order for the Riemannian curvature to vanish, it is necessary to have

$$\partial_t[e_2, e_3] = [\partial_t e_2, e_3] + [e_2, \partial_t e_3], \tag{22}$$

and this equality leads to

$$(e_2\gamma)_x - \beta_x T_x + \gamma_x S_x = 0 \tag{23}$$

Given that g preserves its form under the flow V, the rates of change of the strains S and T imposing equations (18)-(22) are found in [7] to be

$$S_t = \partial_t g_{12} = (\alpha + \beta S + \gamma T)S_x + \beta_x + e_2\alpha + e_2\gamma T \tag{24}$$

$$T_t = \partial_t g_{13} = (\alpha + \beta S + \gamma T)T_x + \gamma_x + e_3\alpha - e_2\gamma S. \tag{25}$$

The terms $e_2\alpha$ and $e_3\alpha$ represent reptation, a rigid sliding of filaments longitudinally along their lengths. We ignore these possibilities for now and consider the

somewhat simplified expressions

$$S_t = \partial_t g_{12} = (\alpha + \beta S + \gamma T)S_x + \beta_x + e_2\gamma T \tag{26}$$

$$T_t = \partial_t g_{13} = (\alpha + \beta S + \gamma T)T_x + \gamma_x - e_2\gamma S \tag{27}$$

2.3 Phenomenological Energy and Interior Forces

Suppose the cilium has length L. Then the energy E of a filament with a given shape is defined as the sum of the shear energy and the bending energy for that shape. As a physical concept, the bending energy of a smooth parameterized curve is defined as the integral with respect to arc length of the curvature squared. Thus, the bending energy E_B is, by definition

$$E_B = \int_0^L (S_x^2 + T_x^2)^2 dx. \tag{28}$$

The shear energy, E_S, is the energy obtained due to the shearing of the filaments and is defined as

$$E_S = \int_0^L ((S-F)^2 + (T-G)^2)dx, \tag{29}$$

where F and G are strains that would minimize the shear energy at a fixed time if attained as values for S and T respectively. The fact that E_S is defined using quadratic terms in S and T reflects the observation that E_S depends on the amount of shearing, but not on the direction of the shear itself.

If μ is the shear modulus (the rigidity) of the ciliary material and κ_c is the bending modulus, then the expression for total energy is

$$E = \frac{\mu}{2}\int_0^L ((S-F)^2 + (T-G)^2)dx + \frac{\kappa_c}{2}\int_0^L (S_x^2 + T_x^2)dx \tag{30}$$

The variational derivatives of this energy with respect to the shear components S and T give the internal stresses Φ and Ψ (see Appendix B):

$$\Phi = \frac{\delta E}{\delta S} = \mu(S - F) - \kappa_c S_{xx}$$
$$\Psi = \frac{\delta E}{\delta T} = \mu(T - G) - \kappa_c T_{xx}.$$

The internal stresses Φ and Ψ associated with S and T are changes in the bending energy of the cilium. These are functions of position measured in units of force and can be determined at a fixed point in time using the equations of continuum mechanics.

Equations (18) and (23) impose inextensibility constraints. To find stresses conjugate to the shear strain, we use the Lagrange multipliers λ and ν. Thus, from [7],

$$E' = E + \int_0^L \lambda(\alpha_x + S\beta_x + T\gamma_x)dx + \int_0^L \nu((e_2\gamma)_x - T_x\beta_x + S_x\gamma_x)dx.$$

One can find the interior forces on the cilium by taking the variational derivative of E' with respect to α, β, and γ [7].

The cilium also experiences exterior forces, which are due to the action of the fluid in which it is immersed. The dissipation function corresponding to those forces is defined by Gueron and Liron [3] as

$$D = \int_0^L \left(\frac{C_T}{2}(\alpha + \beta S + \gamma T)^2 + \frac{C_N}{2}(\beta^2 + \gamma^2) + \frac{C_\omega}{2}(e_2\gamma)^2 \right) dx$$

where C_N, C_T and C_ω are material constants that represent resistance coefficients. Let ω be defined as

$$\omega(x) = e_2\lambda(x),$$

where ω represents the angular velocity, the rate at which e_2 moves towards e_3.

Then the equilibrium condition that interior and exterior forces are equal leads to the following system:

$$C_T(\alpha + \beta S + \gamma T) = -\Phi S_x - \Psi T_x + \lambda_x \tag{31}$$

$$C_N\beta = \Phi_x + \lambda S_x - (\nu T_x)_x \tag{32}$$

$$C_N\gamma = \Phi_x + \lambda T_x + (\nu S_x)_x \tag{33}$$

$$C_\omega\omega = \nu_x - \Phi T + \Psi S \tag{34}$$

After some calculations [7], it is possible to find the equations for λ and ν

$$\lambda_{xx} = \frac{C_T}{C_N}\kappa^2\lambda + (\Phi S_x + \Psi T_x)_x + \frac{C_T}{C_N}(S_x\Phi_x + T_x\Psi_x) + \frac{C_T}{C_N}\tau\kappa^2\nu \tag{35}$$

$$\nu_{xx} = (\Phi T - \Psi S)_x - \frac{C_\omega}{C_N}(S_x\Psi_{xx} - T_x\Phi_{xx} + \lambda\tau\kappa^2 + T_x(\nu T_x)_x x + S_x(\nu S_x)_{xx}) \tag{36}$$

So the complete system describing ciliary motion is:

$$C_T(\alpha + \beta S + \gamma T) = -\Phi S_x - \Psi T_x + \lambda_x$$

$$C_N\beta = \Phi_x + \lambda S_x - (\nu T_x)_x$$

$$C_N\gamma = \Phi_x + \lambda T_x + (\nu S_x)_x$$

$$C_\omega e_2\gamma = \nu_x - \Phi T + \Psi S$$

$$S_t = \partial_t g_{12} = (\alpha + \beta S + \gamma T)S_x + \beta_x + e_2\gamma T$$

$$T_t = \partial_t g_{13} = (\alpha + \beta S + \gamma T)T_x + \gamma_x - e_2\gamma S$$

$$\lambda_{xx} = \frac{C_T}{C_N}\kappa^2\lambda + (\Phi S_x + \Psi T_x)_x + \frac{C_T}{C_N}(S_x\Phi_x + T_x\Psi_x) + \frac{C_T}{C_N}\tau\kappa^2\nu$$

$$\nu_{xx} = (\Phi T - \Psi S)_x - \frac{C_\omega}{C_N}(S_x\Psi_{xx} - T_x\Phi_{xx} + \lambda\tau\kappa^2 + T_x(\nu T_x)_x x + S_x(\nu S_x)_{xx})$$

$$\kappa = \sqrt{S_x^2 + T_x^2}.$$

The most important fact to be noted about this model is that it can reconstruct the motion of the filament at any moment in time using only the expressions for S and T, without any assumption about the shape of the cilium. Thus, shear strain determines bending and no additional assumptions are needed.

In the following sections, we will continue to explore this idea in order to create a numerical simulation of the mathematical model. However, before proceeding, it may be useful to perform one final analytic check on the net force physical constraint.

2.4 The Net Force Condition

Since the cilium cannot exert a net force on itself, it is important to verify that all three cartesian components of the net force will give 0 by integration. This fact has, in fact, been used to determine equations (31) -(34), but the proof may not be obvious from the equations in the model. The calculation is particularly useful because it can also be performed as a check of the numerical method and hence can be used to find errors in programming when the equations are solved using a numerical package such as Matlab.

One should note that this equation of motion is only valid for a cilium that swims freely and is not attached to another body at any of its two ends. If an attachment exists, then it is possible for the cilium to exert a net force on the fluid, which is, for example, the case in the human airway cilia [4]. In this situation, the capacity to exert a net force is in fact the primary mechanism which allows these organelles to perform their function. If there is no attachment, then the shape of the cilium alone determines motion within the fluid. This situation is compatible with the idea that the geometry of the cilium is sufficient to provide an accurate description of its translation and rotation within a fluid.

We proceed by performing the analytic check that the net force integrates to 0.

To obtain the three cartesian components, denoted by F_1, F_2 and F_3, let e_{1k}, e_{2k} and e_{3k} represent the projections of the vectors e_1, e_2 and e_3 along the x direction for $k = 1$, the y direction for $k = 2$ and the z direction for $k = 3$ respectively. The following relations are known:

$$
\begin{aligned}
S_t &= (\alpha + \beta S + \gamma T)S_x + \beta_x + e_2\alpha + \omega T \\
C_T(\alpha + \beta S + \gamma T) &= -\Phi S_x - \Psi T_x + \lambda_x \\
C_N\beta &= \Phi_x + \lambda S_x - (\nu T_x)_x \\
C_N\gamma &= \Psi_x + \lambda T_x + (\nu S_x)_x \\
\partial_x e_2 &= -\kappa \cos\phi e_1 \\
\partial_x e_3 &= -\kappa \sin\phi e_1.
\end{aligned}
$$

We impose the boundary conditions

$$
\begin{aligned}
\Phi(0) = \Phi(L) &= 0 \\
\Psi(0) = \Psi(L) &= 0 \\
\lambda(0) = \lambda(L) &= 0 \\
\nu(0) = \nu(L) &= 0
\end{aligned}
$$

where L is the length of a filament. These conditions are direct consequences of the laws of Newtonian mechanics. For example, λ, which represents tension, must be zero at the endpoints because there is no pulling on the ends of the cilium.

The force F is defined as:

$$
F = (-\Phi S_x - \Psi T_x + \lambda_x)\, e_1 + (\Phi_x + \lambda S_x - (\nu T_x)_x)\, e_2 + (\Psi_x + \lambda T_x + (\nu S_x)_x)\, e_3
$$

so for $k \in \{1, 2, 3\}$,

$$\begin{aligned}
\int_0^L F_k dx &= \int_0^L \left(-\Phi S_x - \Psi T_x + \lambda_x\right) e_{1k} dx + \int_0^L \left(\Phi_x + \lambda S_x - (\nu T_x)_x\right) e_{2k} dx \\
&+ \int_0^L \left(\Psi_x + \lambda T_x + (\nu S_x)_x\right) e_{3k} dx. \\
&= \int_0^L \left(-\Phi S_x - \Psi T_x\right) e_{1k} + \Phi_x e_{2k} + \Psi_x e_{3k} dx \\
&+ \int_0^L \lambda_x e_{1k} + \lambda S_x e_{2k} + \lambda T_x e_{3k} dx + \int_0^L -(\nu T_x)_x e_{2k} + (\nu S_x)_x e_{3k} dx
\end{aligned}$$

It is straightforward to show that each of the three integrals in the sum equals 0 with the appropriate boundary conditions.

$$\begin{aligned}
&\int_0^L \left(-\Phi S_x - \Psi T_x\right) e_{1k} + \Phi_x e_{2k} + \Psi_x e_{3k} dx \\
&= \int_0^L \left(-\Phi\kappa\cos\phi - \Psi\kappa\sin\phi\right) e_{1k} + \Phi_x e_{2k} + \Psi_x e_{3k} dx \\
&= \int_0^L \Phi e_{2k_x} + \Psi e_{2k_x} + \Phi_x e_{2k} + \Psi_x e_{3k} dx \\
&= \int_0^L \left(\Phi e_{2k}\right)_x dx + \int_0^L \left(\Psi e_{3k}\right)_x dx \\
&= \Phi e_{2k}\Big|_0^L + \Psi e_{3k}\Big|_0^L = 0
\end{aligned}$$

$$\begin{aligned}
&\int_0^L \lambda_x e_{1k} + \lambda S_x e_{2k} + \lambda T_x e_{3k} dx \\
&= \int_0^L \lambda_x e_{1k} + \lambda\kappa\cos\phi e_{2k} + \lambda\kappa\sin\phi e_{3k} dx \\
&= \int_0^L \lambda_x e_{1k} + \lambda e_{1k_x} dx \\
&= \int_0^L (\lambda e_{1k})_x dx \\
&= \lambda e_{1k}\Big|_0^L = 0
\end{aligned}$$

$$
\begin{aligned}
&\int_0^L -(\nu T_x)_x e_{2k} + (\nu S_x)_x e_{3k} dx \\
&= \int_0^L -(\nu\kappa \sin\phi)_x e_{2k} + (\nu\kappa\cos\phi)_x e_{3k} dx \\
&= -\nu\kappa \sin\phi e_{2k}\Big|_0^L + \int_0^L \nu\kappa\sin\phi e_{2k_x} dx \\
&+ \nu\kappa\cos\phi e_{3k}\Big|_0^L - \int_0^L \nu\kappa\cos\phi e_{3k_x} dx \\
&= \int_0^L \nu\kappa\sin\phi e_{2k_x} dx + \nu\kappa\cos\phi e_{3k_x} dx \\
&= \int_0^L \nu\kappa\sin\phi(-\kappa\cos e_{1k}) dx + \nu\kappa\cos\phi(-\kappa\sin e_{1k}) dx \\
&= 0
\end{aligned}
$$

Therefore, the integral of the net force is shown to be 0 analytically.

Having performed this final verification, the focus can be now shifted to solving the equations describing the ciliary motion. These numerical solutions provide a basis for creating a computer simulation of the motion. In order to calculate them, we employ the finite element least squares projection method, which is described in some detail in the next section.

3 Numerical Approximations - Finite Elements Methods

Finite element methods are numerical algorithms for solving partial differential equations that require dividing the domain into a finite number of subregions. The goal is to choose this partition in such a way that it becomes possible to approximate given functions up to a desired degree of accuracy on each element of the partition and then to "reconnect" these approximations, subject to some conditions, in order to provide an approximation over the entire domain. Even though the choice of ap-

proximation may vary, all finite elements methods follow the same general principle of dividing the domain and then reconstructing the function [9].

In the least squares finite elements method, the estimation of a function f is done by finding a new function g such that the L^2 distance between f and g, in other words the functional $\int_I (f-g)^2 dx$, is minimal. Other constraints can be imposed, such as boundary conditions, continuity constraints, or requiring g to equal f at some of the points. The primary advantage of the least squares methods is that they lead to symmetric, positive definite linear systems that are easily solved by computational packages.

In this work, the approximating function g is required to have the form of a piecewise polynomial of fixed degree N, that is, g has to be a piecewise function for which all pieces are polynomials of degree N for a fixed value of N. This type of estimation is a particularly important tool in numerical analysis, because the functions it produces have many desirable properties: they can be made continuous and as "smooth" as necessary (one can require continuity of derivatives up to any order), they are flexible in terms of imposing boundary conditions, and, most importantly, they can be easily studied using numerical packages. We proceed by describing the projection method, as well as the resulting linear system.

3.1 Least Squares Projection into Piecewise Polynomial Spaces

Let I be a finite interval of the form $[a, b]$ and choose a partition of I with breakpoints

$$a = b_0 < b_1 < b_2 \cdots < b_{N-1} < b_N = b. \tag{37}$$

A function $PP : I \to R$ is said to be a piecewise polynomial if it is a polynomial

on each subinterval $U_j = [b_{j-1}, b_j]$.

We define V_J to be the space of all piecewise polynomials on the interval I of degree at most J. Similarly, we define V_J^0 as the subspace of V_J consisting of functions which are continuous at the interior breakpoints, and V_J^1 as the subspace of V_J^0 consisting of functions with continuous first derivatives at the interior breakpoints. An element of V_J has the general form

$$PP(x) = \sum_{j=1}^{N} \sum_{i=1}^{J+1} \chi_j \, c_{ij} (x - b_{j-1})^{J-i+1} \,, \tag{38}$$

where χ_j represents the characteristic function of the partition element U_j, and c_{ij}, $i = 1 \ldots J+1$ are the coefficients of the polynomial piece in the subinterval U_j, such that c_{1j} is the coefficient corresponding to the leading term and c_{J+1j} is the coefficient corresponding to the constant term. We compute the following limits:

$$\lim_{x \uparrow b_k} PP(x) = \sum_{i=1}^{J+1} c_{i,k} (b_k - b_{k-1})^{J-i+1} \tag{39}$$

$$\lim_{x \downarrow b_k} PP(x) = c_{J+1,k+1} \tag{40}$$

$$\lim_{x \uparrow b_k} PP'(x) = \sum_{i=1}^{J} (J - i + 1) c_{i,k} (b_k - b_{k-1})^{J-i} \tag{41}$$

$$\lim_{x \downarrow b_k} PP'(x) = c_{J,k+1} \tag{42}$$

To project a function f into the piecewise polynomial space V_J^0 using the least squares method, we minimize the expression

$$\begin{aligned} F[\{c_{ij}\}, \{\lambda_k\}] = & \frac{1}{2} \int_{b_0}^{b_N} [f(x) - PP(x)]^2 \, dx \\ & + \sum_{k=1}^{N-1} \lambda_k \left(\sum_{i=1}^{J+1} c_{i,k} (b_k - b_{k-1})^{J-i+1} - c_{J+1,k+1} \right) , \end{aligned}$$

where λ_k, $k = 1, \ldots N-1$ are Lagrange multipliers used to enforce the $N-1$ continuity

constraints at the breakpoints.

Then the critical point of F must satisfy the condition:

$$\begin{aligned}
0 = \frac{\partial F}{\partial c_{k\ell}} &= \int_{U_\ell} \left[\sum_{i=1}^{J+1} c_{i\ell}(x - b_{\ell-1})^{J-i+1} - f(x) \right] (x - b_{\ell-1})^{J-k+1}\, dx \\
&+ \lambda_\ell (b_\ell - b_{\ell-1})^{J-k+1} - \lambda_{\ell-1}\delta_{k,J+1} \\
&= \sum_{i=1}^{J+1} \int_{U_\ell} c_{i\ell}(x - b_{\ell-1})^{2J-i-k+2}\, dx - \int_{U_\ell} f(x)(x - b_{\ell-1})^{J-k+1}\, dx \\
&+ \lambda_\ell (b_\ell - b_{\ell-1})^{J-k+1} - \lambda_{\ell-1}\delta_{k,J+1}
\end{aligned}$$

Let f_{kl} be defined as

$$f_{kl} = \int_{U_\ell} f(x)(x - b_{\ell-1})^{J-k+1}\, dx\,. \tag{43}$$

Then

$$\frac{\partial F}{\partial c_{k\ell}} = \sum_{i=1}^{J+1} \frac{(b_\ell - b_{\ell-1})^{2J-i-k+3}}{2J - i - k + 3} c_{i\ell} - f_{k\ell} + \lambda_\ell (b_\ell - b_{\ell-1})^{J-k+1} - \lambda_{\ell-1}\delta_{k,J+1}. \tag{44}$$

Thus the critical point is obtained by setting the expression in equation (44) equal to 0. This is equivalent to solving the inhomogeneous linear system:

$$\begin{pmatrix} A & B \\ B^T & 0 \end{pmatrix} \begin{pmatrix} c \\ \lambda \end{pmatrix} = \begin{pmatrix} f \\ 0 \end{pmatrix} \tag{45}$$

where

$$A_{k\ell,ij} = \delta_{\ell j} \frac{(b_\ell - b_{\ell-1})^{2J-i-k+3}}{2J - i - k + 3} \tag{46}$$

$$B_{k\ell,j} = \delta_{\ell j}(b_\ell - b_{\ell-1})^{J-k+1} - \delta_{k,J+1}\delta_{\ell,j+1} \tag{47}$$

The $N-1$ equations in the second row of equation (45) are the continuity constraints at the interior breakpoints.

Example 3.1.

Suppose the chosen interval is $I = [0, 1]$ with breakpoints

$$(b_0, b_1, b_2) = \left(0, \frac{1}{2}, 1\right),$$

and the degree of the polynomials in the desired space is $J = 2$. Let the function f be

$$f(x) = \sin x.$$

Then equation (44) becomes

$$0 = \frac{\partial F}{\partial c_{k\ell}} = \sum_{i=1}^{3} \frac{(b_\ell - b_{\ell-1})^{7-i-k}}{7-i-k} c_{i\ell} - f_{k\ell} + \lambda_\ell (b_\ell - b_{\ell-1})^{3-k} - \lambda_{\ell-1}\delta_{k,3},$$

where

$$f_{k1} = \int_0^{\frac{1}{2}} f(x) \cdot x^{3-k}\, dx\,.$$
$$f_{k2} = \int_{\frac{1}{2}}^{1} f(x) \cdot \left(x - \frac{1}{2}\right)^{3-k} dx\,.$$

Thus,

$$f_{11} = \sin\left(\frac{1}{2}\right) + \frac{3}{4}\cos\left(\frac{1}{2}\right) - 2 \approx 0.15190219$$
$$f_{21} = \sin\left(\frac{1}{2}\right) - \frac{1}{2}\cos\left(\frac{1}{2}\right) \approx 0.04063426$$
$$f_{31} = 1 - \cos\left(\frac{1}{2}\right) \approx 0.1224174$$
$$f_{12} = \frac{7}{4}\cos(1) + \sin(1) - 2\cos\left(\frac{1}{2}\right) \approx 0.03183490$$

$$f_{22} = \sin(1) - \cos(1) + \frac{\cos(1)}{2} - \sin\left(\frac{1}{2}\right) + \frac{1}{2}\cos\left(\frac{1}{2}\right) + \frac{\cos\left(\frac{1}{2}\right)}{2} \approx 0.09189429$$
$$f_{32} = \cos\left(\frac{1}{2}\right) - \cos(1) = 0.3372803$$

The following system is obtained:

$$\begin{aligned}
&\frac{1}{5\cdot 2^5}c_{11} + \frac{1}{4\cdot 2^4}c_{21} + \frac{1}{3\cdot 2^3}c_{31} - f_{11} + \lambda\cdot\frac{1}{4} = 0\\
&\frac{1}{4\cdot 2^4}c_{11} + \frac{1}{3\cdot 2^3}c_{21} + \frac{1}{2\cdot 2^2}c_{31} - f_{21} + \lambda\cdot\frac{1}{2} = 0\\
&\frac{1}{3\cdot 2^3}c_{11} + \frac{1}{2\cdot 2^2}c_{21} + \frac{1}{2}c_{31} - f_{31} + \lambda = 0\\
&\frac{1}{5\cdot 2^5}c_{12} + \frac{1}{4\cdot 2^4}c_{22} + \frac{1}{3\cdot 2^3}c_{32} - f_{12} = 0\\
&\frac{1}{4\cdot 2^4}c_{12} + \frac{1}{3\cdot 2^3}c_{22} + \frac{1}{2\cdot 2^2}c_{32} - f_{22} = 0\\
&\frac{1}{3\cdot 2^3}c_{12} + \frac{1}{2\cdot 2^2}c_{22} + \frac{1}{2}c_{32} - f_{32} - \lambda = 0
\end{aligned}$$

with the continuity constraint

$$\frac{1}{4}c_{11} + \frac{1}{2}c_{21} + c_{31} = c_{32}$$

or equivalently

$$\begin{pmatrix}
\frac{1}{5\cdot 2^5} & \frac{1}{4\cdot 2^4} & \frac{1}{3\cdot 2^3} & 0 & 0 & 0 & \frac{1}{4}\\
\frac{1}{4\cdot 2^4} & \frac{1}{3\cdot 2^3} & \frac{1}{2\cdot 2^2} & 0 & 0 & 0 & \frac{1}{2}\\
\frac{1}{3\cdot 2^3} & \frac{1}{2\cdot 2^2} & \frac{1}{2} & 0 & 0 & 0 & 1\\
0 & 0 & 0 & \frac{1}{5\cdot 2^5} & \frac{1}{4\cdot 2^4} & \frac{1}{3\cdot 2^3} & 0\\
0 & 0 & 0 & \frac{1}{4\cdot 2^4} & \frac{1}{3\cdot 2^3} & \frac{1}{2\cdot 2^2} & 0\\
0 & 0 & 0 & \frac{1}{3\cdot 2^3} & \frac{1}{2\cdot 2^2} & \frac{1}{2} & -1\\
\frac{1}{4} & \frac{1}{2} & 1 & 0 & 0 & -1 & 0
\end{pmatrix}\cdot\begin{pmatrix} c_{11}\\ c_{21}\\ c_{31}\\ c_{12}\\ c_{21}\\ c_{32}\\ \lambda \end{pmatrix} = \begin{pmatrix} f_{11}\\ f_{21}\\ f_{31}\\ f_{21}\\ f_{22}\\ f_{32}\\ 0 \end{pmatrix}$$

Solving this system provides the values for the c coefficients. We have

$$c_{11} \approx -0.1350$$

$$c_{21} \approx 1.0292$$

$$c_{31} \approx -0.0130$$

$$c_{12} \approx -0.3274$$

$$c_{22} \approx 0.8897$$

$$c_{32} \approx 0.4795$$

To demonstrate the accuracy of this method, in figure 3 we plot the sin function on $[0, 1]$ together with its piecewise polynomial approximation.

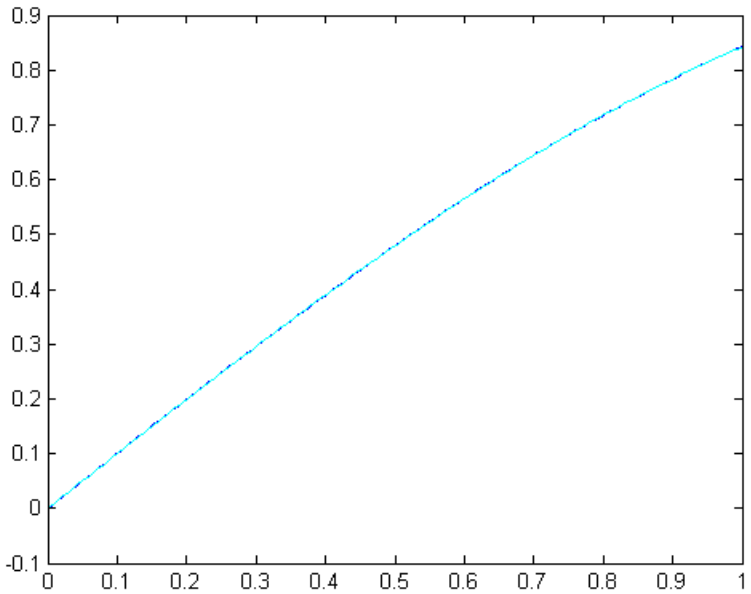

Figure 3: The function $\sin(x)$ (cyan) on [0,1] and its piecewise polynomial approximation on the same interval (blue), obtained by projecting into V_1^0 with one interior breakpoint at $\frac{1}{2}$

Example 3.2.

Suppose f is already a piecewise polynomial, $f \in V_M^0$ for a given M. Then f is of the form

$$f(x) = \sum_{j=1}^{N} \sum_{i=1}^{M+1} \chi_j \, d_{ij} (x - b_{j-1})^{M-i+1} \tag{48}$$

From Eq. (43),

$$f_{k\ell} = \sum_{i=1}^{M+1} d_{i\ell} \frac{(b_\ell - b_{\ell-1})^{M+J-i-k+3}}{M+J-i-k+3} \tag{49}$$

If $M = J$ then $f_{k\ell}$ is simply the identity map in V_J^0, since in this case the polynomials $f_{k\ell}$ are indeed $A_{k\ell,ij} d_{ij}$. If $M < J$, then the projection map is in fact inclusion: the solution to the linear system gives the same polynomial coefficients, but a re-indexing of the terms happens due to the increase in degree. In other words, projecting into a space of higher degree leads to nothing more than a shift in the list of coefficients and a "padding" with additional zeros.

3.2 Projecting in V_J^n

Requiring the least squares piecewise polynomial projection not only to be continuous, but also to have a number of continuous derivatives imposes additional constraints. For instance, one can require the projections to have continuous first derivatives, which is equivalent to projecting the functions into V_J^1. For this problem, we minimize the expression

$$\begin{aligned} F[\{c_{ij}\}, \{\lambda_k\}, \{\mu_k\}] = \frac{1}{2} \int_{b_0}^{b_N} & \left[f(x) - PP(x) \right]^2 \, dx \\ & + \sum_{k=1}^{N-1} \lambda_k \left(\sum_{i=1}^{J+1} c_{i,k} (b_k - b_{k-1})^{J-i+1} - c_{J+1,k+1} \right) \\ & + \sum_{k=1}^{N-1} \mu_k \left(\sum_{i=1}^{J} (J-i+1) c_{ik} (b_k - b_{k-1})^{J-i} - c_{J,k+1} \right), \end{aligned}$$

where λ_k, $k = 1, ...N-1$ are the Lagrange multipliers enforcing the function continuity constraints and μ_k are the Lagrange multipliers enforcing the derivative continuity. The critical point can be found by solving the equation

$$\begin{aligned}
0 = \frac{\partial F}{\partial c_{k\ell}} &= \int_{U_\ell} \left[\sum_{i=1}^{J+1} c_{i\ell}(x - b_{\ell-1})^{J-i+1} - f(x) \right] (x - b_{\ell-1})^{J-k+1} \, dx \\
&+ \lambda_\ell (b_\ell - b_{\ell-1})^{J-k+1} - \lambda_{\ell-1}\delta_{k,J+1} \\
&+ \mu_\ell (J-k+1)(b_\ell - b_{\ell-1})^{J-k} - \mu_{\ell-1}\delta_{k,J} \\
&= \sum_{i=1}^{J+1} \int_{U_\ell} c_{i\ell}(x - b_{\ell-1})^{2J-i-k+2} \, dx - \int_{U_\ell} f(x)(x - b_{\ell-1})^{J-k+1} \, dx \\
&+ \lambda_\ell (b_\ell - b_{\ell-1})^{J-k+1} - \lambda_{\ell-1}\delta_{k,J+1} \\
&+ \mu_\ell (J-k+1)(b_\ell - b_{\ell-1})^{J-k} - \mu_{\ell-1}\delta_{k,J}
\end{aligned}$$

Defining f_{kl} as in Eq. (43), the expression becomes:

$$\begin{aligned}
\frac{\partial F}{\partial c_{k\ell}} = \sum_{i=1}^{J+1} \frac{(b_\ell - b_{\ell-1})^{2J-i-k+3}}{2J-i-k+3} c_{i\ell} - f_{k\ell} + \lambda_\ell (b_\ell - b_{\ell-1})^{J-k+1} - \lambda_{\ell-1}\delta_{k,J+1} \\
+ \mu_\ell (J-k+1)(b_\ell - b_{\ell-1})^{J-k} - \mu_{\ell-1}\delta_{k,J}.
\end{aligned}$$

Hence, the linear system for the V_J^1 projection is:

$$\begin{pmatrix} A & B & C \\ B^T & 0 & 0 \\ C^T & 0 & 0 \end{pmatrix} \begin{pmatrix} c \\ \lambda \\ \mu \end{pmatrix} = \begin{pmatrix} f \\ 0 \\ 0 \end{pmatrix} \tag{50}$$

with

$$\begin{aligned}
A_{k\ell,ij} &= \delta_{\ell j} \frac{(b_\ell - b_{\ell-1})^{2J-i-k+3}}{2J-i-k+3} \\
B_{k\ell,j} &= \delta_{\ell j}(b_\ell - b_{\ell-1})^{J-k+1} - \delta_{k,J+1}\delta_{\ell,j+1}
\end{aligned}$$

$$C_{k\ell,j} = \delta_{\ell j}(J-k+1)(b_\ell - b_{\ell-1})^{J-k} - \delta_{k,J}\delta_{\ell,j+1}.$$

The $N-1$ equations in the second row enforce continuity of the function at the interior breakpoints and the $N-1$ equations in the third row enforce continuity of the first derivative.

In general, the projection into the space V_J^n is analogous to that for the V_J^1 projection, but each additional continuity constraint requires $N-1$ additional equation. Thus, projection in V_J^n entails solving a system of $(n+1)(N-1)$ linear equations. For our purposes, it will suffice to consider spaces V_J^n with $n \leq 4$, since none of the projections employed will require more than four continuous derivatives.

It is also possible to impose additional constraints, such as boundary conditions on the function or one of its derivatives. One natural such condition is asking that the function be held constant at the endpoints. For example, assume that the boundary constraint is that

$$PP(b_0) = PP(b_N) = 0.$$

Therefore,

$$\begin{aligned} &c_{J+1,1} = 0 \\ &\sum_{i=1}^{J+1} c_{i,N}(b_N - b_{N-1})^{J-i+1} = 0, \end{aligned}$$

so it suffices to append these two new equations to the already existing system to obtain the required approximation.

The cases where the derivatives are required to be 0 at endpoints can be treated

in an identical manner.

Example 3.3.

Figure 4 shows the function $f(x) = \sin(x)$ projected into V_4^0, V_4^1, V_4^2 and V_4^3 respectively, with boundary conditions $f(0) = f(\frac{\pi}{2}) = 0$ and 5 breakpoints in the interval. It is important to note that these conditions are highly unnatural, because while $\sin\frac{\pi}{2} = 1$, the projections are forcing the endpoints to stay fixed at 0. Therefore, the projections are forced to oscillate about the $\sin(x)$ line when they approach $\frac{\pi}{2}$ and, as a result, the approximations close to $\frac{\pi}{2}$ are quite inaccurate. The treatment of the boundary constraint, as well as the inaccuracy of the estimation, depend on the amount of continuity expected from the piecewise polynomial space.

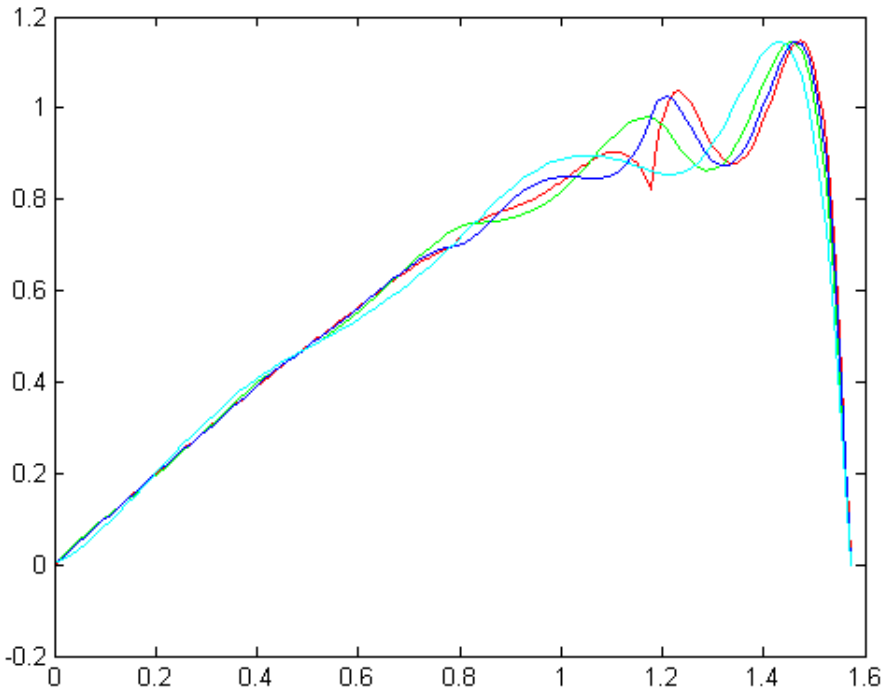

Figure 4: The function $\sin(x)$ projected into the spaces V_4^0 (red), V_4^1 (blue), V_4^2 (green), and V_4^3 (cyan) on the interval $[0, \frac{\pi}{2}]$ with $f(0) = f(\frac{\pi}{2}) = 0$

Example 3.4.

As demonstrated by figure 4, inappropriate boundary conditions can lead to poor approximations, because the function is forced to obey unnatural constraints. This fact is of particular importance in the modeling of ciliary dynamics, because boundary conditions often appear in the equations that are to be solved to determine the motion of the organelle.

One other issue to be addressed is that of continuity. It is to be expected that projecting a discontinuous function into a space of continuous piecewise polynomials may cause problems with the approximation as it attempts to fit discontinuities. For instance, let g be the projection of a function f in V_J^0 and consider the derivative of g. Since continuous differentiability is not required in V_J^0, g' may be discontinuous. Projecting g' into V_J^0 again is an example of fitting a discontinuous function by a continuous piecewise polynomial.

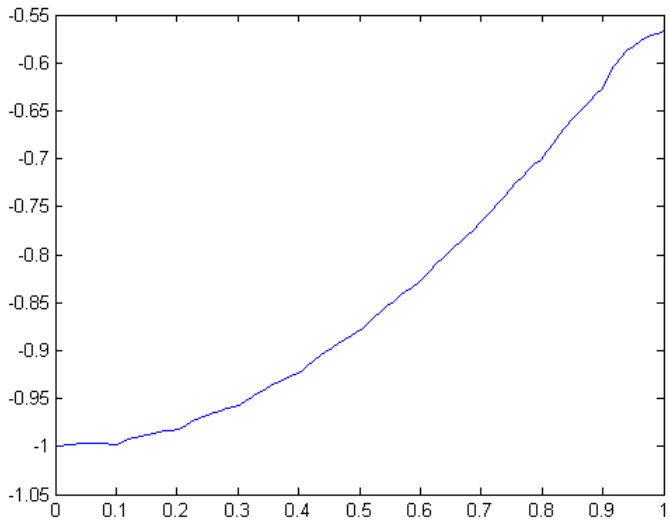

Figure 5: The repetition of the process of projecting $\sin(x)$ into V_3^0, differentiating the result and then re-projecting it into V_3^0 leads to poor approximations about the breakpoints and endpoints, as shown by the projection obtained for $-\cos(x)$ after three iterations

In figure 5, the function $\sin(x)$ is projected into V_3^0 with 10 equally spaced breakpoints on [0,1]. The resulting piecewise polynomial is differentiated (thus producing an estimation of $\cos(x)$) and the resulting function is then projected back into V_3^0. The process is repeated three times, until an estimation of $-\cos(x)$ is obtained. Even after three iterations, the discontinuity issues become visible at the breakpoints. What is more, the endpoints estimation is particularly far from the actual value.

Repeating the process once more in order to obtain a V_3^0 approximation for $\sin(x)$ shows that iterated projections into unsuitable spaces can be highly irregular and unpredictable (figure 6).

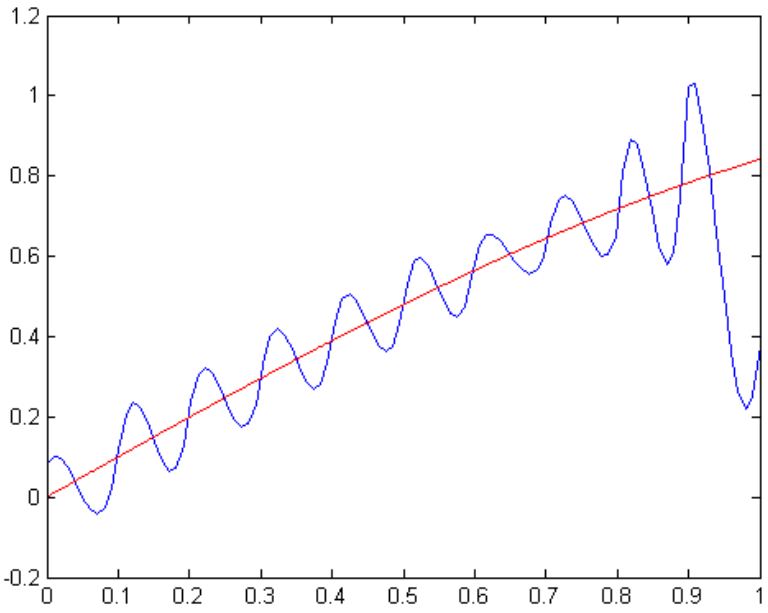

Figure 6: If the process of projecting, differentiating and re-projecting is repeated once more after the estimate for $-\cos(x)$ is obtained, then the approximation for $\sin(x)$ that should be obtained is in fact very inaccurate. The approximating piecewise polynomial is plotted in blue, and the actual sin function is plotted in red

It is important to note that throughout this analysis no condition has been put on the partitioning of the interval $[b_0, b_N]$, although for all the examples the breakpoints were chosen to be equally spaced. This choice is not arbitrary, but motivated by the literature on piecewise polynomial least squares projections: in [2], Dubeau proves that the best least squares piecewise n degree polynomial approximation is obtained for the uniform partition. Thus, after using this result implicitly, we now establish the formal rule that, for our approximations, the intervals $[b_k, b_{k+1}]$ will always be taken to have constant length $\frac{b_N - b_0}{N}$.

3.3 The Heat Equation

Solving a partial differential equation, such as the heat equation, is a useful test for the least squares projection method. Let u be a function satisfying the equation

$$u_t = u_{xx}, \tag{51}$$

with initial condition

$$u(x, 0) = \sin(\pi x),$$

and boundary conditions

$$u(0, t) = u(1, t) = 0$$

A numerical solution to the equation is based on the approximation

$$u(x, t + \Delta t) \approx u(x, t) + \Delta t u_t(x, t) = u(x, t) + \Delta t u_{xx}(x, t). \tag{52}$$

It is thus possible to "follow" the solution in time, using discrete time points. Projections into the space of piecewise polynomials are particularly useful in this case, because they simplify differentiation. At each time t, the function u is projected

into V_J^n for fixed values of J and n, then the resulting piecewise polynomial is differentiated twice with respect to x, multiplied by the size of the time interval and added to the value of u at t. This algorithm produces $u(x, t + \Delta t)$, which can be used in the next time step. In Figure 7, we show a plot of the solution obtained through this method.

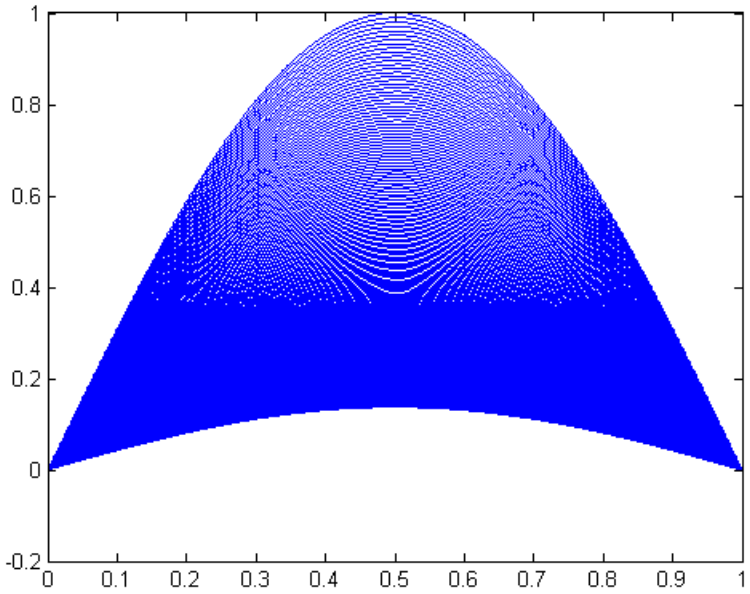

Figure 7: The solution of the heat equation obtained by following the heat function's evolution in time. As expected, the heat tends to equalize along the interval [0,1]

In this case, as in all others, there is no obvious choice for the degree J of the polynomials in the projection space. Clearly, the polynomials should be at least quadratics in order to permit two differentiations, but there is no apparent upper bound on the degree. In fact, since a higher degree gives the system more freedom to approximate functions, it may be expected that high degree piecewise polynomials produce the most accurate approximation of the heat equation solution. However, the numerical simulations show that the opposite is true: projecting into a space of

a high degree polynomials offers unnecessary freedom that can cause problems with the estimation. The reason for this apparent paradox lies in the issue described in example 3.4. If the degree of the space is high, but there are no continuity constraints imposed on the second derivative, then differentiating u twice as required means that u_{xx} may be discontinuous. Attempting to fit discontinuities by a continuous function results in problems that become obvious after the first few iteration. Nevertheless, if the degree of the projection space is low, then the amount of freedom available for fitting discontinuities is sufficiently low so as not to permit too much instability.

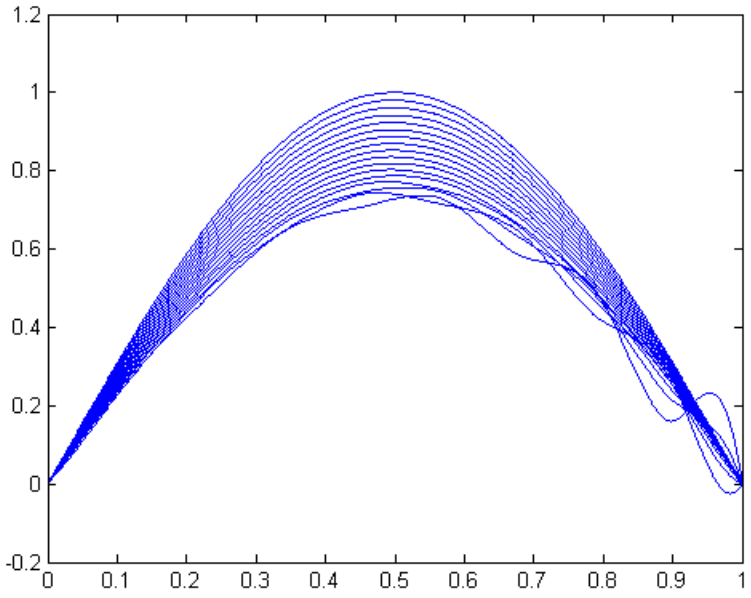

Figure 8: The heat equation solution is highly unstable when the projections are done in the space V_3^1 and the interval is divided into 10 breakpoints

In figure 7, the projections are done in V_2^1, the space of piecewise polynomials of degree 2 with continuous first derivatives, for 10 breakpoints chosen to be equally spaced between 0 and 1. In this case, the solution is stable and exhibits the desired

decaying behavior. It is even possible to plot the numerical solution at a fixed time t on the same graph as the solution obtained through analytical methods to check that the result is accurate and behaves as expected. This outcome is due to the relatively low degree of V_2^1, which, coupled with the continuity condition on the first derivative, does not allow for too much freedom to fit discontinuities in the second derivative. In contrast with the degree 2 case, for the same number of breakpoints (10 equally spaced breakpoints from 0 to 1), projecting into higher degree spaces leads to increasing levels of instability, as shown in figure 8. More

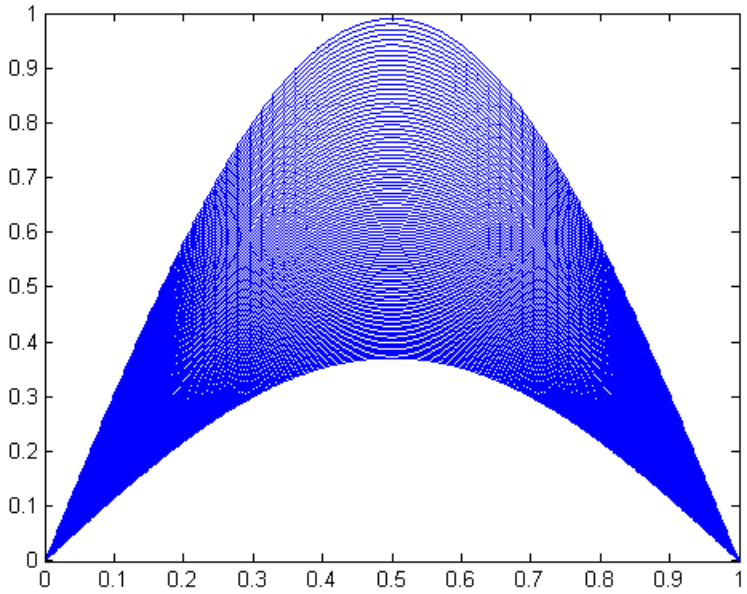

Figure 9: The heat equation solution becomes stable again when the projections are done in the space V_3^1, but the interval is divided into only 5 breakpoints

interestingly perhaps, lowering the number of available breakpoints reintroduces stability even for higher degree projections. As shown in figure 9, if projection in the space of cubic piecewise polynomials with continuous first derivatives is limited to only 5 breakpoints, the numerical solution to the heat equation is, again, stable

and behaves in the usual manner (exhibits uniform decay). Since discontinuities can only occur at the breakpoints (all the V_J spaces contain functions which are at least piecewise continuous), lowering the number of breakpoints means lowering the number of points where continuity issues may occur. For this particular example, dividing the domain into only 5 intervals solves the stability problem.

If the discontinuous second derivative concern disappears (by projection into V_J^2 for suitable values of J), then stability is no longer an issue. The function u is estimated appropriately for any number of breakpoints and any degree (figure 10).

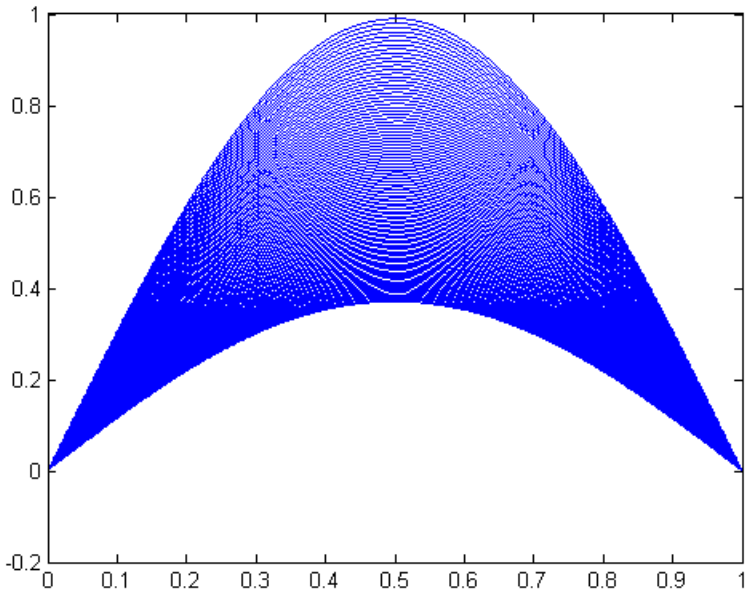

Figure 10: The heat equation solution with projections in $V_1 0^2$. Although the degree of the polynomials is high, requiring the continuity of the second derivative resolves the instability

The conclusion that the heat equation solution estimation leads to is that the number of degrees of freedom available to the system plays a vital role in stability issues. As a result, we find that it is beneficial to choose the lowest possible value

for J which still allows the continuity and differentiability conditions to be satisfied, or, alternatively, to require sufficient continuity and differentiability conditions to limit the degrees of freedom for a given polynomial order J.

3.4 Solving $\Lambda_{xx} = g\Lambda + h$

We now focus on providing a method of solving the equation

$$\Lambda_{xx} = g\Lambda + h. \tag{53}$$

This result will prove useful in the calculation of the shear strain, that depends, among others, on a Lagrange multiplier λ described by an equation of the form above. We restate the problem using the language of the calculus of variations: find $\Lambda \in V_J^0$ that minimizes

$$G = \int_I \left[\frac{1}{2}(\Lambda_x)^2 + \frac{1}{2} g\Lambda^2 + h\Lambda \right] dx\,, \tag{54}$$

i.e. find the critical point of G by solving

$$\frac{\partial G}{\partial c_{kl}} = 0 \tag{55}$$

where $\{c_{kl}\}$ are the coefficients of the piecewise polynomial Λ and the differential equation is subject to suitable constraints. Finding the solution to this problem reduces to solving a linear system similar to that of Eq. (45). In fact, the equations enforcing the continuity constraints required by the V_j^0 projection are the same that coefficient matrix B represents in Eq. (45). The matrix A becomes $A = A^{(1)} + A^{(2)}$ with

$$A^{(1)}_{k\ell,ij} = \delta_{\ell j} \frac{(b_\ell - b_{\ell-1})^{2J-i-k+1}(J-i+1)(J-k+1)}{2J-i-k+1} \tag{56}$$

if $k < J+1$ and $i < J+1$, and 0 otherwise and

$$A^{(2)}_{k\ell,ij} = \delta_{\ell j} \int_{U_\ell} (x - b_{\ell-1})^{2J-i-k+2} g(x)\, dx \tag{57}$$

which is obtained from the moments of the function g. Thus, the linear system to be solved is

$$\begin{pmatrix} A^{(1)} + A^{(2)} & B \\ B^T & 0 \end{pmatrix} \begin{pmatrix} c \\ \lambda \end{pmatrix} = \begin{pmatrix} -h \\ 0 \end{pmatrix} \tag{58}$$

$-h$ is a column vector of the moments $-h_{kl}$ of the function h.

Example 3.5.

We solve the equation with

$$I = [0, 1]$$

$$g(x) = 1$$

$$h(x) = x$$

and boundary conditions

$$\Lambda(0) = \Lambda(1) = 0.$$

For these conditions, the solution can be easily computed analytically and can be compared with the numerical solution.

We have

$$\Lambda(x) = -x + \frac{e^x - e^{-x}}{e - e^{-1}}\,. \tag{59}$$

Figure 11 shows the analytic solution and the variational method solution plotted on the same graph.

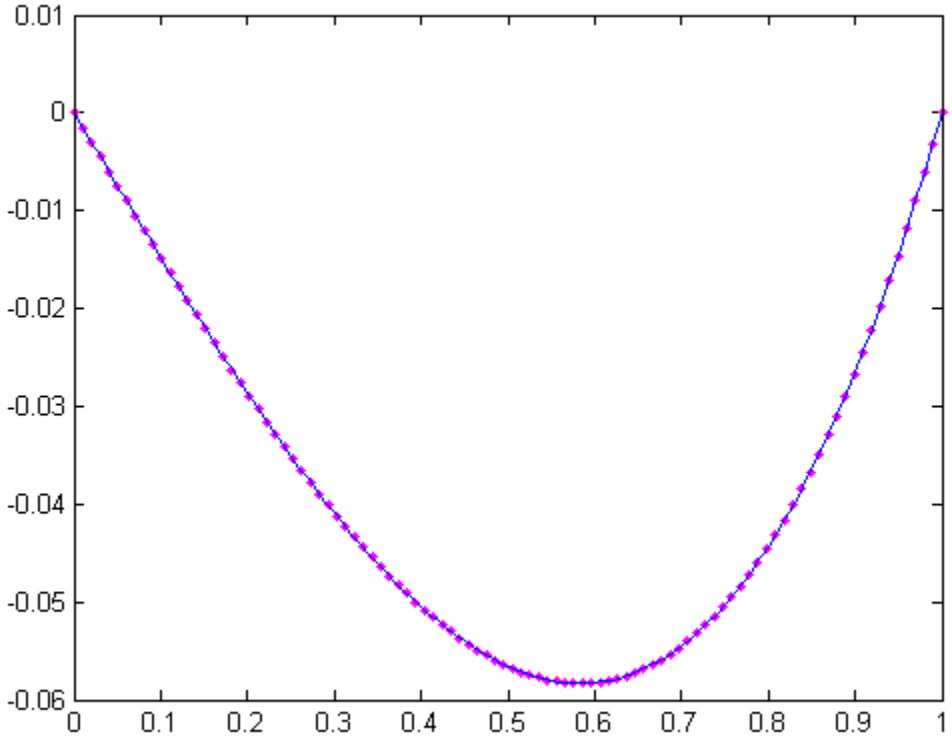

Figure 11: The analytic and the numerical solution of the equation $\Lambda_{xx} = g\Lambda + h$. The dotted line represents the analytic solution, while the solid line is the numerical approximation

Having introduced the method of solving partial differential equations through piecewise polynomial least squares approximations, we now demonstrate how the method can be applied to solving the equations of ciliary motion.

4 Two-dimensional Ciliary Motion

Assume initially that the cilium moves only in a plane. This approach reduces the problem to the two-dimensional case, simplifying the system to be solved. In nature, planar beats are observed in various protozoans, as well as in Ctenophora [1], so the

two dimensional problem is not just a simplification, but also the rendition of an actual biological pattern. In this case, from equation (17), V has the expression

$$V = (\alpha + \beta S)e_1 + \beta e_2$$

We rewrite the system of differential equations that describe the motion, ignoring the terms specific to the third dimension:

$$S_t = (\alpha + \beta S)\, S_x + \beta_x \tag{60}$$

$$C_T(\alpha + \beta S) = -\Phi S_x + \lambda_x \tag{61}$$

$$C_N \beta = \Phi_x + \lambda S_x \tag{62}$$

$$\lambda_{xx} = \frac{C_T}{C_N}\kappa^2 \lambda + (\Phi S_x)_x + \frac{C_T}{C_N} S_x \Phi_x \tag{63}$$

$$\kappa = S_x \tag{64}$$

These identities are equations (24), (31), (33), (35), and (10) reduced to the planar case. The conditions to be followed are

$$C_T = 1$$

$$C_N = 2$$

$$S(x, 0) = 0$$

$$S(0, x) = S(1, x) = 0$$

$$\Phi(x) = \sin(\pi x)\cos(2\pi t)$$

The values chosen for C_T and C_N approximate the constants determined in [8], the expression for $\Phi(x)$ represents a "driving term" which forces the motion, the $S(x, 0) = 0$ condition comes from the assumption that the cilium has no stresses at

the initial time and the $S(0,x) = S(1,x) = 0$ expression represents the condition that the stress should vanish at the endpoints.

To solve these equations numerically, it suffices to project the functions into the space of piecewise polynomials with appropriate continuity conditions and "follow" the evolution of these projections at discrete points in time, as with the heat equation.

After some straightforward manipulations, the system becomes

$$S_t = \frac{-\Phi S_x + \lambda_x}{C_T} S_x + \frac{\Phi_{xx} + \lambda_x S_x + \lambda S_{xx}}{C_N} \tag{65}$$

$$\lambda_{xx} = \frac{C_T}{C_N} S_x^2 \lambda + \Phi_x S_x \left(1 + \frac{C_T}{C_N}\right) + \Phi S_{xx} \tag{66}$$

In spite of the multitude of terms involved, solving these equations does not require any different techniques than those used in the piecewise polynomial projection examples. In fact, the second equation is essentially of the form $\lambda_{xx} = g\lambda + h$, which has already been solved in section 3.4. Solving this equation at a fixed point t in time provides the λ value at t, which can then be used to find the solution to the first equation. In figure 12, we show the estimated evolution of the filament shape as time progresses.

Although the filament moves in a pattern that resembles the experimental data, after a few time steps it becomes clear that the solution does not in fact behave as expected, because the inextensibility constraint is violated: the length of the cilium, assumed to be 1 initially, increases as time passes. One potential reason for this issue may be related to the instability that was also observed when solving the heat equation. It has been shown in section 3.3 that the piecewise polynomial projection can behave unexpectedly for unsuitable choices of the degree, set of breakpoints or continuity requirements. When the projections are iterated, as it happens in the algorithm that produces figure 12, the method can be particularly sensitive to such

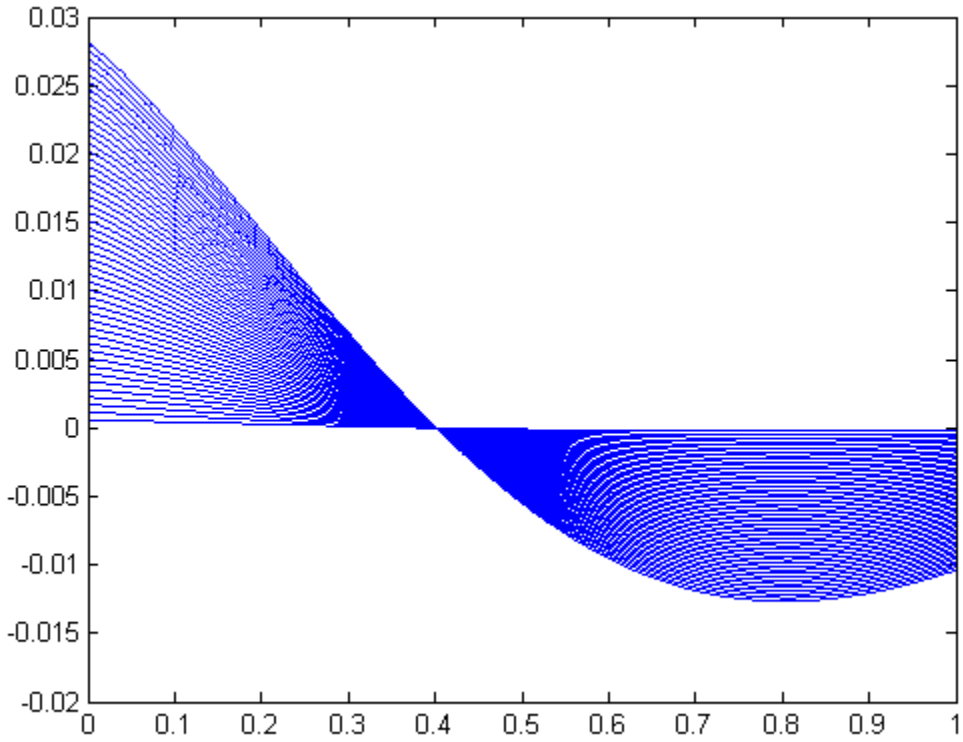

Figure 12: The filament begins as horizontal and bends due to the strain

choices, so it is possible that this may be the cause for the change in filament length.

Although all precautions were taken to project the functions into suitable spaces, it has not been possible to correct the issue by mere changes in degrees or number of breakpoints. This outcome suggests that a different, unknown type of discontinuity may be arising at the breakpoints. Therefore, despite the general good behavior of the projection, before attempting to simulate the three dimensional case, a more detailed analysis of the numerical method should be performed.

In conclusion, this result shows that, although the piecewise polynomial method is suitable for solving the differential equations which describe ciliary motion, there are still challenges to be addressed to ensure stability. Future work should consider

the stability issue in greater detail and perhaps develop a new strategy for solving continuity problems. One potential approach could be to vary the set of breakpoints between time steps so that errors cannot build up at certain points. If two sets of breakpoints are used alternatively, then at any value x the function would be a polynomial, and thus infinitely differentiable, for every other time step. After stability is ensured, graphs and movies of the filament motion can be obtained and compared to biological data. It is expected that these approximations will serve as evidence for the geometric model, which states that for a free flowing cilium, the change in shape is the sole determinant of the translation and rotation pattern.

A Conditions for Ciliary Flows

If the flow V preserves the form of the metric tensor g, then $g_{22} = 1+S^2$, so $\partial_t g_{22} = 2SS_t$; Also, $g_{33} = 1+T^2$, so $\partial_t g_{33} = 2TT_t$ and $g_{23} = ST$, so $\partial_t g_{23} = ST_t + TS_t$. But the change of S in time is given by the change in the component g_{12} and the rate of change of T is given by g_{13}. So we have the following relations

$$\partial_t g_{22} = 2SS_t = 2S\partial_t g_{12}$$

$$\partial_t g_{33} = 2TT_t = 2T\partial_t g_{13}$$

$$\partial_t g_{23} = ST_t + TS_t = S\partial_t g_{13} + T\partial_t g_{12}$$

We perform the necessary calculations:

$$\begin{aligned}
\partial_t g_{22} &= Vg_{22} + 2g([\partial_y, V], \partial_y) \\
&= 2\alpha SS_x + 2g(\alpha_y\partial_x + \beta_y\partial_y + \gamma_y\partial_z, \partial_y) \\
&= 2\alpha SS_x + 2(\alpha_y g(\partial_x, \partial_y) + \beta_y g(\partial_y, \partial_y) + \gamma_y g(\partial_z, \partial_y)) \\
&= 2\alpha SS_x + 2(S\alpha_y + (1+S^2)\beta_y + ST\gamma_y)
\end{aligned}$$

$$\begin{aligned}
\partial_t g_{12} &= Vg_{12} + g([\partial_y, V], \partial_x) + g([\partial_x, V], \partial_y) \\
&= \alpha S_x + g(\alpha_y\partial_x + \beta_y\partial_y + \gamma_y\partial_z, \partial_x) + g(\alpha_x\partial_x + \beta_x\partial_y + \gamma_x\partial_z, \partial_y) \\
&= \alpha S_x + \alpha_y g(\partial_x, \partial_x) + \beta_y g(\partial_y, \partial_x) + \gamma_y g(\partial_z, \partial_x) \\
&+ \alpha_x g(\partial_x, \partial_y) + \beta_x g(\partial_y, \partial_y) + \gamma_x(\partial_z, \partial_y) \\
&= \alpha S_x + \alpha_y + \beta_y S + \gamma_y T + \alpha_x S + \beta_x(1+S^2) + \gamma_x ST \\
&= \alpha S_x + \alpha_y + \beta_y S + \gamma_y T + \beta_x + S(\alpha_x + \beta_x S + \gamma_x T) \\
&= \alpha S_x + \alpha_y + \beta_y S + \gamma_y T + \beta_x
\end{aligned}$$

where the last equality comes from equation (18). So we have that

$$2\alpha S S_x + 2(S\alpha_y + (1+S^2)\beta_y + ST\gamma_y) = 2S(\alpha S_x + \alpha_y + \beta_y S + \gamma_y T + \beta_x)$$

and thus

$$\beta_y - S\beta_x = 0,$$

which is equivalent to $e_2\beta = 0$. Also,

$$\begin{aligned}
\partial_t g_{33} &= V g_{33} + 2g([\partial_z, V], \partial_z) \\
&= 2\alpha T T_x + 2g(\alpha_z\partial_x + \beta_z\partial_y + \gamma_z\partial_z, \partial_z) \\
&= 2\alpha T T_x + 2(\alpha_z g(\partial_x, \partial_z) + \beta_z g(\partial_y, \partial_z) + \gamma_z g(\partial_z, \partial_z)) \\
&= 2\alpha T T_x + 2(T\alpha_z + ST\beta_z + (1+T^2)\gamma_z) \\
\partial_t g_{13} &= V g_{13} + g([\partial_z, V], \partial_x) + g([\partial_x, V], \partial_z) \\
&= \alpha T_x + g(\alpha_z\partial_x + \beta_z\partial_y + \gamma_z\partial_z, \partial_x) \\
&+ g(\alpha_x\partial_x + \beta_x\partial_y + \gamma_x\partial_z, \partial_z) \\
&= \alpha T_x + \alpha_z g(\partial_x, \partial_x) + \beta_z g(\partial_y, \partial_x) \\
&+ \gamma_z g(\partial_z, \partial_x) + \alpha_x g(\partial_x, \partial_z) + \beta_x g(\partial_y, \partial_z) + \gamma_x(\partial_z, \partial_z) \\
&= \alpha T_x + \alpha_z + \beta_z S + \gamma_z T + \alpha_x T + \beta_x ST + \gamma_x(1+T^2) \\
&= \alpha T_x + \alpha_z + \beta_z S + \gamma_z T + \gamma_x + T(\alpha_x + \beta_x S + \gamma_x T) \\
&= \alpha T_x + \alpha_z + \beta_z S + \gamma_z T + \gamma_x
\end{aligned}$$

So as before

$$2\alpha T T_x + 2(T\alpha_z + ST\beta_z + (1+T^2)\gamma_z) = 2T(\alpha T_x + \alpha_z + \beta_z S + \gamma_z T + \gamma_x)$$

and thus

$$\gamma_y = z - T\gamma_x = 0,$$

which is equivalent to $e_3\gamma = 0$.

Finally,

$$\begin{aligned}
\partial_t g_{23} &= Vg_{23} + g([\partial_z, V], \partial_y) + g([\partial_y, V], \partial_z) \\
&= \alpha(ST_x + TSx) + g(\alpha_z\partial_x + \beta_z\partial_y + \gamma_z\partial_z, \partial_y) + g(\alpha_y\partial_x + \beta_y\partial_y + \gamma_y\partial_z, \partial_z) \\
&= \alpha(ST_x + TSx) + \alpha_z g(\partial_x, \partial_y) + \beta_z g(\partial_y, \partial_y) + \gamma_z g(\partial_z, \partial_y) \\
&+ \alpha_y g(\partial_x, \partial_z) + \beta_y g(\partial_y, \partial_z) + \gamma_y(\partial_z, \partial_z) \\
&= \alpha(ST_x + TSx) + \alpha_y S + \beta_y(1 + S^2) + \gamma_y ST + \alpha_y T + \beta_y ST + \gamma_y(1 + T^2),
\end{aligned}$$

which leads to

$$\begin{aligned}
&\alpha(ST_x + TSx) + \alpha_y S + \beta_y(1 + S^2) + \gamma_y ST + \alpha_y T + \beta_y ST + \gamma_y(1 + T^2) \\
&= S(\alpha T_x + \alpha_z + \beta_z S + \gamma_z T + \gamma_x) + T(\alpha S_x + \alpha_y + \beta_y S + \gamma_y T + \beta_x).
\end{aligned}$$

so

$$\gamma_y - S\gamma_x + \beta_z - T\beta_x = 0,$$

and, equivalently $e_2\gamma + e_3\beta = 0$.

B Variational Derivatives of Elastic Energy

The variational derivative is an important tool in the calculus of variations. Intuitively, the variational derivative of a functional F with respect to its argument f indicates how much F changes due to an infinitesimal change in f, denoted by δf. To find the variational derivative of E with respect to S, where

$$E = \frac{\mu}{2}\int_0^L ((S-F)^2 + (T-G)^2)dx + \frac{\kappa_c}{2}\int_0^L (S_x^2 + T_x^2)dx,$$

suppose S varies by a small amount δS. Define $\tilde{S} = S + \delta S$, which leads to

$$\tilde{E} = \frac{\mu}{2}\int_0^L ((S+\delta S-F)^2 + (T-G)^2)dx + \frac{\kappa_c}{2}\int_0^L ((S_x+\delta S_x)^2 + T_x^2)dx,$$

Then δE, also known as the first variation of E is given by

$$\begin{aligned}\delta E &= \tilde{E} - E \\ &= \frac{\mu}{2}\int_0^L (2\delta S(S-F) + \delta S^2)dx + \frac{\kappa_c}{2}\int_0^L (2S_x\delta S_x + (\delta S_x)^2)dx\end{aligned}$$

Since δS is small, $(\delta S)^2$ can be considered an error term and subsequently ignored. Through integration by parts, applying the natural boundary condition $S_x(0) = S_x(L) = 0$,

$$\begin{aligned}\delta E &= \mu\int_0^L \delta S(S-F)dx + \kappa_c\int_0^L S_x\delta S_x dx \\ &= \mu\int_0^L \delta S(S-F)dx + \kappa_c S_x\delta S\Big|_0^L - \kappa_c\int_0^L S_x x\delta S dx \\ &= \mu\int_0^L \delta S(S-F)dx - \kappa_c\int_0^L S_x x\delta S dx\end{aligned}$$

Then

$$\frac{\delta E}{\delta S} = \mu(S - F) - \kappa_c S_x x.$$

Through an identical calculation, imposing boundary conditions $T_x(0) = T_x(L) = 0$, it also results that

$$\frac{\delta E}{\delta T} = \mu(T - G) - \kappa_c T_x x.$$

References

[1] Bourne G., Cytology and Cell Physiology, 4th edition, Academic Press, San Diego, CA (1987), pp. 404

[2] Dubeau F., Uniform Partitioning and the Best Least-Squares Piecewise Polynomial Approximation, Bull. Austral. Math. Soc, Vol 44 (1991), pp. 279–283

[3] Gueron S. and Liron N., Simulations of Three-Dimensional Ciliary Beats and Cilia Interactions, Biophys. J., Vol 65 (1993), pp. 499–507

[4] Hill D. et. al., Force Generation and Dynamics of Individual Cilia under External Loading, Biophys. J, Vol 98 (2010), pp. 57–66

[5] Karp G., Cell and Molecular Biology: Concepts and Experiments, 6th ed., John Wiley and Sons (2009) pp. 340

[6] Lodish H. et. al., Molec. Cell Bio., 4th ed., W.H. Freeman, New York (2000)

[7] Peterson M., Geometry of Ciliary Dynamics, Phys. Rev. E, Vol 80 (2009), 011923

[8] Peterson M. et. al., Internal Stress Analysis of a Ciliary Beat, Mount Holyoke College REU report (2010)

[9] Zienkiewicz, O. C., et.al. The finite element method: its basis and fundamentals, 6th ed., Butterworth-Heinemann, Burlington, MA (2005)